genes

Article

HEATR3 as a Potential Biomarker in Head and Neck Squamous Cell Carcinoma: Transcriptomic Identification and Validation in Oral Squamous Cell Carcinoma

Giovanni Tossetta [1,*], Magdalena Smolik [2] and Roberto Campagna [1]

[1] Department for the Promotion of Human Science and Quality of Life, San Raffaele Roma University, Via di Val Cannuta, 247, 00166 Rome, Italy; roberto.campagna@uniroma5.it
[2] Department of Toxicology, Jagiellonian University Medical College, Medyczna 9, Kraków 30-688, Poland; magdalena.smolik@uj.edu.pl
* Correspondence: giovanni.tossetta@uniroma5.it

Abstract

Background: HEAT repeat-containing protein 3 (*HEATR3*) participates in ribosome biogenesis and nucleolar stress responses, but its clinical and molecular relevance in head and neck squamous cell carcinoma (HNSCC) and oral squamous cell carcinoma (OSCC) remains poorly characterized. This study investigated *HEATR3* expression, prognostic significance, and associated molecular networks in TCGA-HNSC, with independent transcriptomic validation in oral squamous cell carcinoma (OSCC). **Methods**: *HEATR3* expression and its association with clinical outcomes were investigated using TCGA-HNSC data. Survival analyses included Kaplan–Meier estimates and multivariable Cox regression. Tumor microenvironment correlations, functional enrichment, and protein interaction networks were examined using TIMER3, GEPIA3, STRING, BioGRID, and R-based analyses. *HEATR3* expression was independently evaluated in GEO datasets GSE37991 and GSE30784. **Results**: *HEATR3* expression was significantly elevated in TCGA-HNSC tissues compared with non-cancerous controls. High *HEATR3* expression was associated with poorer overall survival (OS), and this association persisted after adjustment for clinicopathological variables. An association with progression-free interval (PFI) was observed in unadjusted analyses but was not retained following multivariable adjustment. *HEATR3*-associated genes were enriched in ribosome biogenesis and RNA-processing functions, while correlations with stromal cell abundance varied across deconvolution methods. Independent OSCC analyses showed increased *HEATR3* expression with both probes in GSE37991, whereas only one of two probes demonstrated significant upregulation in GSE30784. **Conclusions**: *HEATR3* is transcriptionally upregulated in TCGA-HNSC, with additional but probe-dependent evidence of increased expression in independent OSCC cohorts. Higher *HEATR3* expression is also associated with poorer OS in TCGA-HNSC. Its molecular associations with RNA metabolism and ribosome biogenesis support further investigation of *HEATR3* as a potential prognostic biomarker.

Keywords: *HEATR3*; OSCC; KEGG; STRING; TCGA-HNSC; head and neck squamous cell carcinoma; HNSCC; oral squamous cell carcinoma

Academic Editor: Massimiliano Chetta

Received: 1 November 2026
Revised: 16 November 2026
Accepted: 17 November 2026
Published: 18 November 2026

Copyright: © 2026 by the authors. Licensee MDPI, Basel, Switzerland. This article is an open access article distributed under the terms and conditions of the Creative Commons Attribution (CC BY) license.

1. Introduction

Head and neck squamous cell carcinoma (HNSCC) includes a heterogeneous group of epithelial malignancies arising from the mucosal surfaces of the oral cavity, pharynx, and larynx [1]. These tumors represent a substantial clinical burden worldwide, with considerable differences in incidence, etiological factors, and clinical outcomes according to anatomical location and geographic region [2–4]. Tobacco smoking and alcohol consumption remain major risk factors, particularly for cancers of the oral cavity and larynx, whereas persistent infection with high-risk human papillomaviruses (HPVs) is strongly associated with a distinct subset of oropharyngeal carcinomas [5–8]. Oral squamous cell carcinoma (OSCC), one of the major HNSCC subtypes, may develop through progressive alterations of the oral epithelium, including premalignant changes and epithelial dysplasia [9–12]. Despite advances in surgical management, radiotherapy, systemic treatments, and immunotherapy, disease recurrence and unfavorable outcomes continue to affect a substantial proportion of patients, emphasizing the importance of improving molecular characterization and prognostic stratification [13–16].

Among the cellular processes frequently altered in cancer, ribosome biogenesis has attracted increasing attention because of its close relationship with proliferative activity, metabolic adaptation, and cellular stress responses [17,18]. Ribosome production requires the coordinated transcription and processing of ribosomal RNAs (rRNAs), the synthesis and nuclear import of ribosomal proteins, and the assembly of ribosomal subunits [19]. These events are tightly integrated with signaling pathways that regulate cell growth and protein synthesis. Cancer cells frequently exhibit increased ribosomal biogenesis and altered translational regulation, which can support the production of proteins required for proliferation, survival, and adaptation to changing environmental conditions [20–22]. Importantly, ribosome biogenesis is also connected to tumor-suppressive mechanisms through nucleolar surveillance pathways that respond to disturbances in ribosomal assembly and influence p53 stability [23].

HEAT repeat-containing protein 3 (*HEATR3*) has emerged as a component of the molecular machinery involved in ribosome biogenesis. It has been demonstrated that *HEATR3* contributes to the nuclear accumulation of the large-subunit ribosomal protein uL18 (RPL5) and to processes required for pre-rRNA maturation and ribosomal subunit assembly [24]. Biallelic pathogenic variants affecting *HEATR3* have been associated with Diamond-Blackfan anemia, providing evidence of its physiological importance in maintaining ribosomal homeostasis [25]. Additional studies have implicated *HEATR3* in the nucleolar surveillance pathway, particularly in mechanisms linking ribosomal stress to the stabilization of p53 [24]. Other HEAT repeat-containing proteins have also been implicated in cancer-associated molecular processes. HEATR1, a nucleolar protein involved in ribosome biogenesis, has been shown to promote OSCC cell proliferation by stabilizing the Pontin/Reptin complex and regulating mTOR signaling and pre-rRNA synthesis [26]. In hepatocellular carcinoma, HEATR1 contributes to tumor growth through the regulation of ribosome biogenesis and proteome homeostasis [27]. Beyond the HEATR proteins, the HEAT-repeat-containing scaffold protein PPP2R1A has been implicated in endometrial cancer, where recurrent mutations affecting its HEAT-repeat regions alter PP2A complex function and promote tumor cell growth [28]. These findings indicate that HEAT repeat-containing proteins participate in different cancer-associated molecular processes, although their specific functions and contributions to tumor biology are protein-dependent. Moreover, these observations establish a biological connection between *HEATR3*, ribosome assembly, and cellular stress signaling, although the implications of these functions for malignant transformation and tumor progression remain to be defined.

In the present study, we investigated *HEATR3* using an integrated bioinformatics approach based on publicly available transcriptomic, genomic, and clinical data. *HEATR3* expression was examined in TCGA-HNSC samples, and its association with overall survival (OS) and progression-free interval (PFI) was evaluated through Kaplan–Meier and Cox regression analyses, including adjustment for relevant clinicopathological variables. Genomic alterations, relationships with tumor microenvironment components, functional enrichment of co-expressed genes, and protein interaction networks were also investigated. Finally, *HEATR3* expression was independently evaluated in two GEO datasets, GSE37991 and GSE30784, to assess the reproducibility of its expression pattern in OSCC. Through these complementary analyses, we aimed to characterize the molecular and clinical associations of *HEATR3* in HNSCC and explore its potential as a prognostic biomarker.

2. Materials and Methods

2.1. HEATR3 Expression in TCGA-HNSC Tumors

HEATR3 expression differences in TCGA-HNSC tumor samples (N = 520) and 44 TCGA adjacent non-tumor sample tissues (N = 44) were investigated using Gene Expression Profiling Interactive Analysis version 3 (GEPIA3) (https://gepia3.bioinfoliu.com, accessed on 20 September 2026) webserver [29]. Expression levels were reported as log2(TPM + 1).

The GEPIA3 "Stage Plot" function was used to visualize the distribution of *HEATR3* expression across pathological stages I–IV (Stage I, N = 27; Stage II, N = 81; Stage III, N = 93; Stage IV, N = 318). Differences in mean *HEATR3* expression among the four groups were assessed using one-way analysis of variance (ANOVA).

Overall survival (OS) and progression-free interval (PFI) analyses were conducted using R statistical software (version 4.6.1; R Foundation for Statistical Computing, Vienna, Austria), as previously described [30].

Briefly, patients were divided into two groups (*HEATR3*-low and *HEATR3*-high) using the median *HEATR3* expression level across the TCGA-HNSC cohort as the cutoff. Survival curves were compared using the log-rank test. PFI data were obtained from the standardized TCGA Pan-Cancer Clinical Data Resource (TCGA-CDR), developed by Liu et al. [31], using the corresponding PFI event indicators and follow-up times.

Multivariable Cox proportional hazards regression models were initially fitted to evaluate the association between *HEATR3* expression and the hazard of death (OS) or a PFI event, adjusting for age at diagnosis, sex, and pathological stage. Associations were expressed as hazard ratios (HRs) with corresponding 95% confidence intervals (CIs).

Age was included as a continuous variable, whereas pathological stages were grouped into early (stages I–II) and advanced (stages III–IV) disease.

Additional multivariable models included anatomical tumor site as a covariate, with human papillomavirus (HPV) status used for stratification in separate models. Anatomical tumor-site information was obtained from a patient-level TCGA-HNSC dataset and linked to the expression and clinical data using TCGA patient identifiers. Tumors were classified into oral cavity, oropharyngeal, and laryngeal groups. The oral cavity group included tumors annotated as alveolar ridge, buccal mucosa, floor of mouth, hard palate, lip, oral cavity, and oral tongue. The oropharyngeal group included base of tongue, oropharynx, and tonsil. Two hypopharyngeal cases were excluded from site-adjusted analyses because of their insufficient representation. Pathological stages were considered separately as stages I, II, III, and IV, with stages IVA, IVB, and IVC combined into stage IV. Stage I and the oral cavity were used as reference categories. Of the 519 patients with available *HEATR3* expression and survival data, 444 had complete information on age, sex, and pathological stage and were eligible for the corresponding multivariable models. Anatomical tumor-site information was available for 279 patients. After excluding two hypopharyngeal cases and 38 patients with missing or non-classifiable pathological stage

information, 239 patients remained eligible for site-adjusted analyses. To assess potential selection bias, demographic and clinicopathological characteristics were compared between included and excluded patients using the Wilcoxon rank-sum test for age, the chi-squared test for sex and pathological stage, and Fisher's exact test for anatomical-site distribution among patients with available and eligible site annotations. The number of events and median follow-up were calculated for each survival analysis, with median follow-up estimated using the reverse Kaplan–Meier method. Additional Cox regression models were fitted to evaluate the stability of *HEATR3*-associated overall survival estimates across analytical populations.

HPV status for survival analyses was obtained from the `Final_HPV_Status` variable in the original TCGA-HNSC patient-level data and matched to expression and clinical data using TCGA patient identifiers. The final analytical population comprised 239 patients, including 216 HPV-negative and 23 HPV-positive cases. HPV-stratified Cox regression models were fitted using the 'strata(HPV)' function to allow different baseline hazards according to HPV status. The proportional hazards assumption was evaluated using Schoenfeld residual-based tests for individual covariates and the overall models.

Survival probabilities and the associations between *HEATR3* expression and clinical outcomes were analyzed using the R package 'survival', which provides functions for Kaplan–Meier estimation and Cox regression. Survival curves were generated using 'survminer' and 'ggplot2', two R packages for graphical visualization. Adjusted hazard ratios (HRs) and their 95% confidence intervals (CIs) were displayed using forest plots generated with 'ggplot2' and 'forestplot'. Survival curves included the number of patients at risk over time, with follow-up expressed in years.

All statistical tests were considered statistically significant at $p < 0.05$.

2.2. Tumor Microenvironment Cell Infiltration Analysis

Correlations between *HEATR3* expression and estimated cancer-associated fibroblast and endothelial-cell abundance were evaluated using the TIMER3 Gene module, as previously reported [30]. The analyses included the overall TCGA-HNSC cohort and the HPV-positive and HPV-negative subgroups defined by TIMER3. Cell abundance estimates were obtained using TIDE, EPIC, xCell, MCP-counter, and ConsensusTME, according to their availability for each cell population. Correlations were assessed using the platform's tumor purity-adjusted partial Spearman correlation framework, which accounts for estimated tumor purity as a potential confounding factor. Correlation coefficients (ϱ) and nominal statistical significance were obtained directly from TIMER3.

For HPV-specific tumor microenvironment analyses, the subgroup classifications provided by TIMER3 were used. These analyses included 421 HPV-negative and 97 HPV-positive tumors, corresponding to 518 of the 520 tumors in the overall cohort. These platform-defined groups were analyzed independently of the clinically annotated population used for survival analyses.

2.3. HEATR3-Related Gene Ontology and KEGG Pathway Enrichment Analyses

To investigate the biological processes and molecular pathways associated with *HEATR3* expression in head and neck squamous cell carcinoma TCGA-HNSC, the top 100 genes positively correlated with *HEATR3* were retrieved from the TCGA-HNSC dataset using the GEPIA3 (version 3) "Expression Network" module. Gene co-expression was assessed using Pearson correlation coefficients based on 520 primary tumor samples. The resulting gene list was subjected to Gene Ontology (GO) and Kyoto Encyclopedia of Genes and Genomes (KEGG) pathway enrichment analyses using R (version 4.6.1).

Gene annotations were processed using the AnnotationDbi and org.Hs.eg.db packages. Ensembl gene identifiers were converted into Entrez Gene identifiers, and ambiguous

annotations were resolved according to the original gene symbols. To define an appropriate background for the enrichment analyses, RNA-sequencing expression data from the 520 primary tumors in TCGA-HNSC were used. Genes were considered expressed if they exhibited TPM ≥ 1 in at least 10% of tumor samples. This filtering procedure identified 21,008 expressed Ensembl gene identifiers, of which 17,448 could be mapped to Entrez Gene identifiers. The mapping procedure identified 179 Ensembl identifiers associated with multiple Entrez identifiers, resulting in 17,610 distinct Entrez Gene identifiers after duplicate removal. These identifiers were used to define the background universe for functional enrichment analysis. Of the original 100 *HEATR3*-correlated genes, 98 fulfilled the expression and annotation criteria and were retained for enrichment analysis.

Functional enrichment analyses were performed using the clusterProfiler package. GO over-representation analysis was conducted separately for Biological Process (BP), Cellular Component (CC), and Molecular Function (MF) categories using the enrichGO function. KEGG pathway enrichment analysis was performed using enrichKEGG, specifying the human organism (hsa). The expressed-gene background was supplied as the reference universe for both analyses. Gene sets containing fewer than 10 or more than 500 annotated genes were excluded, according to the default size thresholds implemented in clusterProfiler. These limits were used to reduce the influence of sparsely annotated gene sets and overly broad functional categories and were applied independently of the size of the 98-gene input list. Statistical significance was assessed using the Benjamini–Hochberg procedure to correct for multiple testing, and terms or pathways with adjusted p-values < 0.05 were considered statistically significant.

GO enrichment results were visualized using horizontal bar plots displaying statistically significant terms from the three ontologies, with enrichment significance expressed as −log10(adjusted p-value). KEGG pathway results were visualized using bubble plots displaying the top 10 pathways ranked by nominal p-value. KEGG findings were interpreted according to their Benjamini–Hochberg-adjusted significance levels. All graphical representations were generated using ggplot2.

2.4. Protein–Protein Interaction Analysis of HEATR3-Related Genes

The STRING database (https://cn.string-db.org, accessed on 25 September 2026) was used to investigate protein associations among the top 100 genes positively correlated with *HEATR3* expression in TCGA-HNSC, identified using GEPIA3. STRING analysis was performed as previously reported [30]. STRING integrates evidence from multiple sources, including experimental studies, curated databases, co-expression analyses, and computational predictions. The resulting network was interpreted as a protein association network rather than evidence of direct physical interactions between all connected proteins.

2.5. HEATR3–Protein Interaction Analysis

The BioGRID database (version 5.0.262) (https://thebiogrid.org, accessed on 22 September 2026) was used to investigate experimentally reported interactions involving *HEATR3*. BioGRID curates interactions from published studies and classifies the supporting evidence according to the experimental approaches used. Because experimentally reported associations may represent indirect interactions or reflect biological contexts other than TCGA-HNSC, the resulting network was interpreted as a reference interaction map rather than a tumor-specific *HEATR3* interactome.

2.6. Validation of HEATR3 Expression in OSCC Independent Cohorts

The differential expression of *HEATR3* was independently evaluated using two publicly available Gene Expression Omnibus (GEO) datasets, GSE30784 and GSE37991. Processed expression matrices and association sample metadata were downloaded using the GEOquery (v. 2.80.0) package in R. The main characteristics of both datasets are summarized in Table 1.

Table 1. Characteristics of the GEO datasets used for *HEATR3* expression validation.

	GSE37991	**GSE30784**
Platform accession	GPL6883	GPL570
Microarray platform	Illumina HumanRef-8 v3.0 Expression BeadChip	Affymetrix Human Genome U133 Plus 2.0 Array
Total samples	80	229
OSCC samples	40	167
Non-tumor/normal samples	40	45
Oral dysplasia samples	0	17
Study design	Forty paired tumor and non-tumor samples	Independent control, dysplasia, and OSCC samples
Expression data processing	Quantile normalization and log2 transformation	gcRMA normalization (log2 scale)

GSE37991 included 40 OSCC specimens and 40 non-tumor oral epithelial samples, organized into 40 matched pairs according to the GEO sample identifiers. Expression data had previously undergone quantile normalization and were log2-transformed before analysis. Two probes corresponding to *HEATR3*, originally annotated as FLJ20718 (ILMN_1666082 and ILMN_1808219), were identified using the platform annotation and the corresponding Entrez Gene ID (55027).

GSE30784 comprised 229 specimens, including 167 OSCC samples, 17 oral dysplasia samples, and 45 normal controls. Expression values had been processed using the GC Robust Multi-array Average (gcRMA) algorithm and were already available on a log2 scale. Accordingly, no additional transformation or normalization was applied. Samples were classified into the three groups according to their GEO metadata. Two probes corresponding to *HEATR3* (1554478_a_at and 219289_at) were identified using the GPL570 annotation.

Differential expression analyses were performed using the limma package (v. 3.68.5) in R. For GSE37991, a paired linear model incorporating patient identifiers was applied to compare OSCC specimens with their corresponding non-tumor tissues. For GSE30784, a linear model for independent groups was fitted, followed by three predefined comparisons: OSCC versus Control, Dysplasia versus Control, and OSCC versus Dysplasia. Linear models were fitted across all microarray probes, and differential expression was assessed using empirical Bayes-moderated t-tests. Patient identifiers were included in the GSE37991 model to account for the paired study design, whereas independent-group comparisons were performed for GSE30784. Differential expression was quantified as the log2 fold change (log2FC), with corresponding 95% confidence intervals. *p*-values were adjusted for multiple testing using the Benjamini–Hochberg procedure, applied across all probes separately for each comparison. An adjusted p-value < 0.05 was considered statistically significant. Graphical representations were generated using ggplot2 (v. 4.0.3).

Both *HEATR3*-associated probes were evaluated in each dataset to assess probe-level consistency. The ILMN_1808219 probe was used for the main visualization of GSE37991, whereas the 1554478_a_at probe was used for GSE30784. Expression distributions were visualized using boxplots with individual sample values. For GSE37991, paired observations were connected to illustrate within-patient differences, and a heatmap was generated to display *HEATR3* expression across the matched specimens.

3. Results

3.1. HEATR3 Expression Across Normal Human Tissues and Cell Populations

To characterize the physiological expression profile of *HEATR3*, its transcript levels were examined across normal human tissues and cell populations using publicly available transcriptomic data. Analysis of tissue-level RNA expression showed a broad distribution of *HEATR3*, with low tissue specificity (Figure 1A). The highest *HEATR3* expression levels were observed in the appendix, skeletal muscle, lymph nodes, tongue, and tonsils. Notably, *HEATR3* expression was detected in the tongue and other tissues anatomically relevant to HNSCC and OSCC, including the salivary glands and esophagus. Single-cell RNA expression analysis further confirmed the widespread distribution of *HEATR3* across different cellular populations, with low cell-type specificity (Figure 1B). The highest expression was observed in mononuclear phagocytes, followed by smooth muscle cells, neuronal cells, and natural killer cells. *HEATR3* transcripts were also detected in squamous epithelial cells, including those from the tongue and esophagus, albeit at lower levels than in several immune cell populations. Thus, *HEATR3* is broadly expressed in normal human tissues, including epithelial populations relevant to HNSCC and OSCC, as well as immune cell populations that may contribute to its overall expression in tumor specimens.

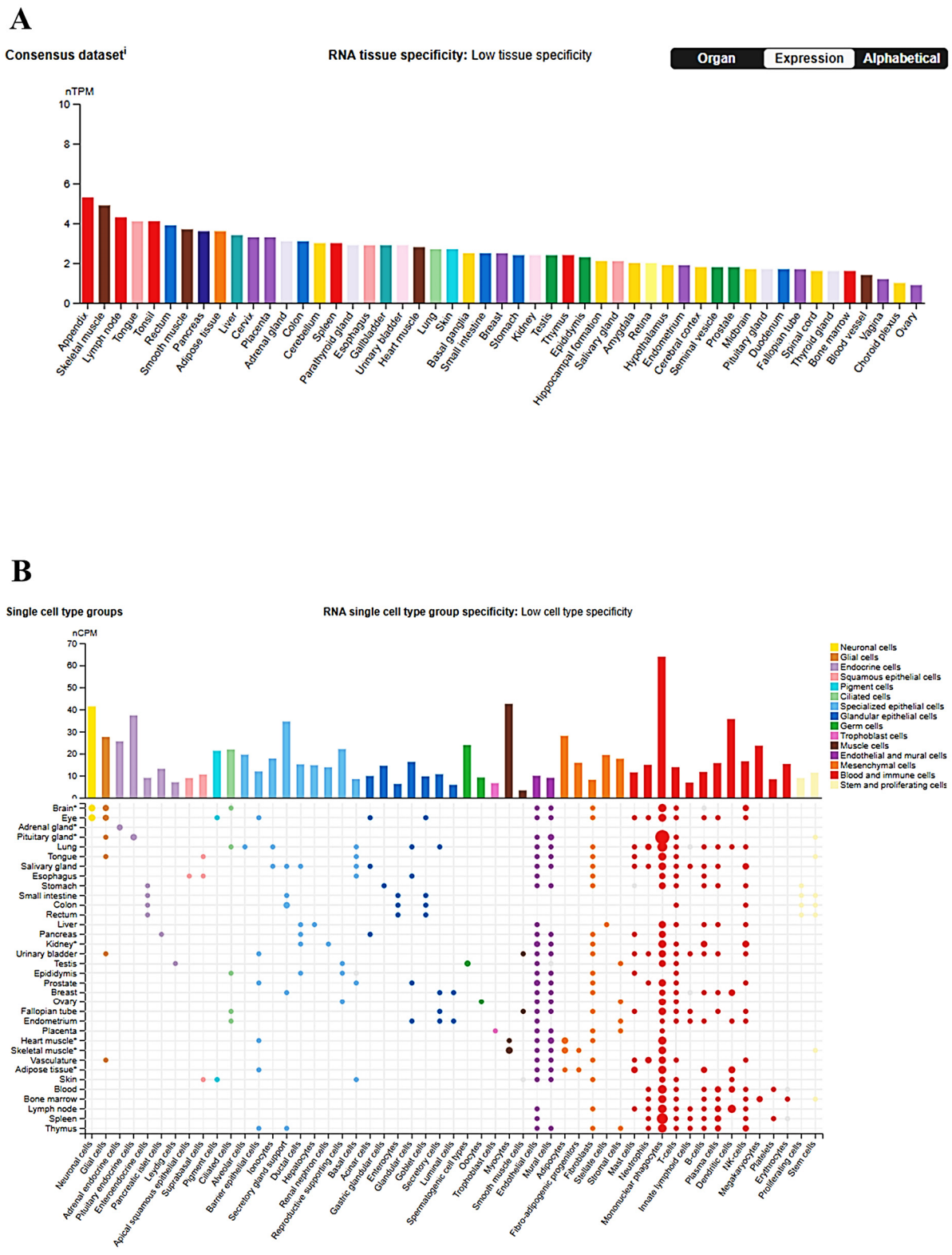


Figure 1. *HEATR3* RNA expression across normal human tissues and cell types. (**A**) *HEATR3* expression across normal human tissues based on the Human Protein Atlas consensus dataset. Expression levels are reported as normalized transcripts per million (nTPM). (**B**) Single-cell RNA expression of *HEATR3* across different cell populations, expressed as normalized counts per million (nCPM).

3.2. HEATR3 Expression in TCGA-HNSC and Its Association with Pathological Stage

In order to investigate the potential involvement of *HEATR3* in TCGA-HNSC, we compared its mRNA expression levels between normal and tumor tissues. As shown in Figure 2A, *HEATR3* expression was significantly higher in TCGA-HNSC tumor samples than in adjacent non-tumor tissues ($p = 3.8 \times 10^{-5}$), although the expression distributions showed considerable overlap between the two groups. To further investigate whether *HEATR3* expression was associated with tumor progression, we analyzed its expression levels in TCGA-HNSC patients across pathological stages I-IV. As shown in Figure 2B, no statistically significant differences were found across stages ($p = 0.1$). These findings show that *HEATR3* expression is upregulated in TCGA-HNSC compared to normal tissues, whereas no statistically significant differences were detected across pathological stages.

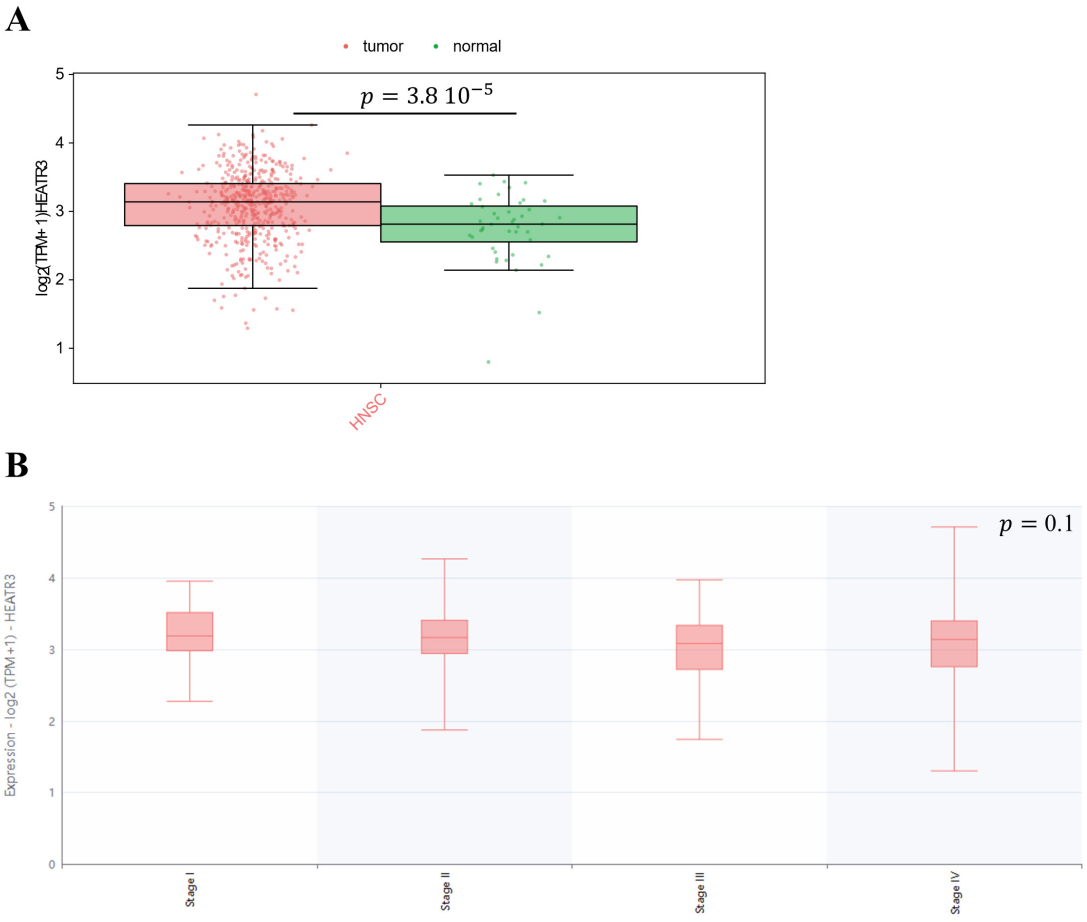


Figure 2. *HEATR3* expression in TCGA-HNSC samples. (**A**) Comparison of *HEATR3* mRNA expression between TCGA-HNSC tissues (N = 520; red) and TCGA adjacent non-tumor tissues (N = 44, green). The *X*-axis indicates tissue type, while the *Y*-axis represents *HEATR3* expression as log2(TPM + 1). (**B**) Distribution of *HEATR3* mRNA expression across pathological stages I–IV in TCGA-HNSC patients. TPM, transcripts per million; HNSC, head and neck squamous cell carcinoma; TCGA, The Cancer Genome Atlas.

3.3. Genomic Alterations of HEATR3 in TCGA-HNSC and OSCC

In order to evaluate possible *HEATR3* genomic alterations in TCGA-HNSC and OSCC, publicly available genomic data were analyzed using cBioPortal. As reported in Figure 3, in the TCGA-HNSC PanCancer Atlas cohort, *HEATR3* alterations were detected in 0.96% of cases, predominantly consisting of gene amplifications (0.57%) and somatic mutations (0.38%) (Figure 3A). In contrast, no *HEATR3* mutations were detected in the MD Anderson Cancer Discovery 2013 OSCC cohort, comprising 40 samples, for which copy-number alteration data were not available (Figure 3A). However, the limited cohort size precludes definitive conclusions regarding the occurrence of rare *HEATR3* mutations in OSCC. Further characterization of *HEATR3* mutations in the TCGA-HNSC cohort showed two missense variants (p.S402C and p.R665Q), affecting amino acid residues 402 and 665, respectively (Figure 3B). However, both variants were classified as variants of uncertain significance (VUS), suggesting that the increased *HEATR3* expression found in tumor tissues is unlikely to be primarily explained by recurrent somatic mutations or high-level gene amplifications.

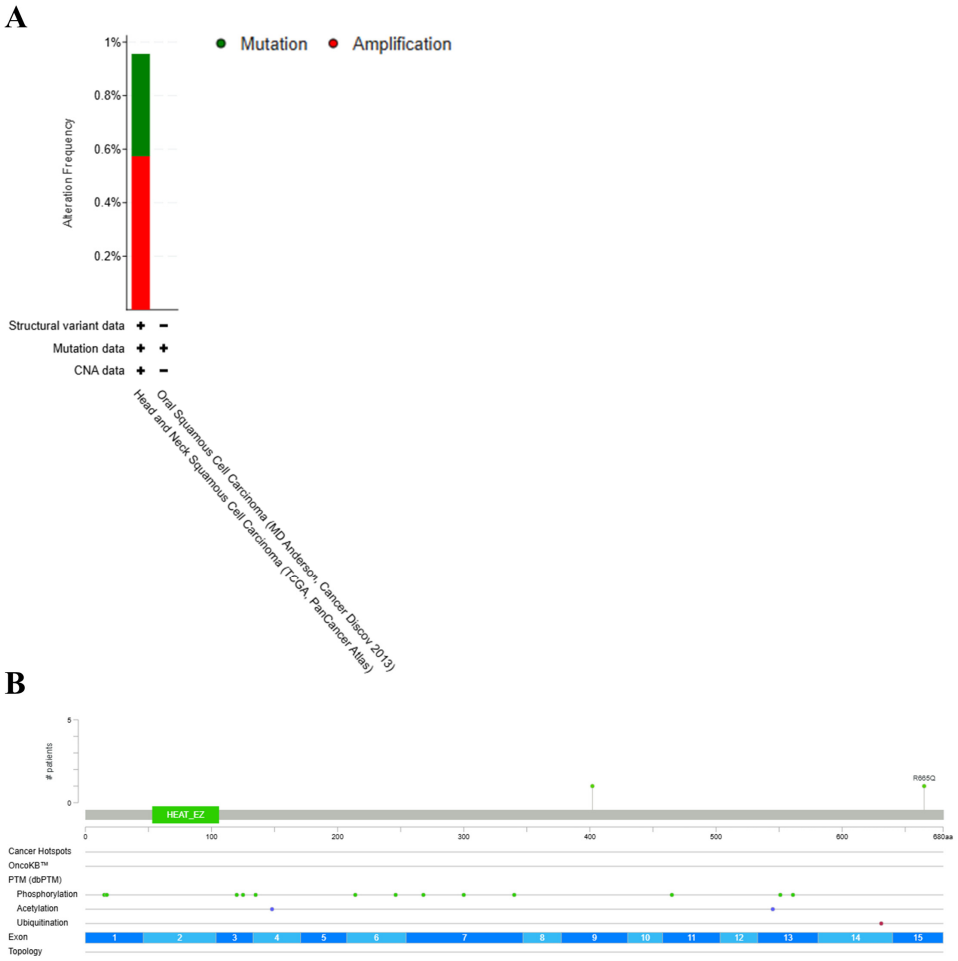


Figure 3. Genomic alterations of *HEATR3* in TCGA-HNSC and OSCC. (**A**) Frequency and distribution of *HEATR3* genomic alterations across the TCGA-HNSC PanCancer Atlas and MD Anderson Cancer Discovery 2013 OSCC cohorts, analyzed using cBioPortal. Alterations are categorized as somatic mutations (green) or gene amplifications (red). The availability of structural variant, mutation, and copy-number alteration (CNA) data is indicated below each cohort. (**B**) Lollipop plot showing the distribution of somatic mutations along the *HEATR3* protein sequence in the TCGA-HNSC cohort. The HEAT_EZ domain, protein exon structure, and post-translational modification sites annotated in dbPTM and displayed through cBioPortal, including phosphorylation, acetylation, and

ubiquitination, are also shown. These annotations provide general protein sequence information and do not represent post-translational modifications experimentally identified in the analyzed TCGA-HNSC samples.

3.4. Association of HEATR3 Expression with Overall Survival and Progression-Free Interval in TCGA-HNSC

The prognostic relevance of *HEATR3* expression was investigated in the TCGA-HNSC cohort by evaluating overall survival (OS) and progression-free interval (PFI). Patients were classified into *HEATR3*-low and *HEATR3*-high groups according to the median expression value. As shown in Figure 4A, Kaplan–Meier analysis revealed significantly poorer OS in patients with high *HEATR3* expression compared with those exhibiting low expression (HR = 1.53, 95% CI 1.17–2.00; log-rank p = 0.0018). Similarly, high *HEATR3* expression was associated with a significantly shorter PFI (HR = 1.37, 95% CI 1.03–1.81; log-rank p = 0.029; Figure 4B).

To determine whether these associations persisted after accounting for relevant clinicopathological variables (age, sex, pathological stage, and anatomical tumor site), multivariable Cox regression analyses were performed. As reported in Figure 4C, high *HEATR3* expression remained significantly associated with poorer OS (adjusted HR = 1.626, 95% CI 1.123–2.354; p = 0.01). Increasing age was also associated with a higher mortality hazard (HR = 1.026 per year, 95% CI 1.008–1.044; p = 0.0038), whereas sex, pathological stage, and anatomical site did not show statistically significant associations with OS. To account for potential differences in baseline hazards according to HPV status, an additional HPV-stratified Cox regression analysis was performed. The association between high *HEATR3* expression and poorer OS remained statistically significant (adjusted HR = 1.616, 95% CI 1.113–2.345; p = 0.0116; Figure 4D). In this model, increasing age (HR = 1.026, 95% CI 1.008–1.043; p = 0.0042) and pathological stage IV compared with stage I (HR = 3.519, 95% CI 1.078–11.482; p = 0.037) were also associated with higher mortality hazards. Contrarily, the association between *HEATR3* expression and PFI observed in the unadjusted analysis was no longer statistically significant after multivariable adjustment (HR = 1.185, 95% CI 0.782–1.798; p = 0.42; Figure 4E). Similarly, the HPV-stratified Cox model did not identify a significant association between *HEATR3* expression and PFI (HR = 1.168, 95% CI 0.768–1.777; p = 0.47; Figure 4F). None of the other clinicopathological variables showed statistically significant associations with PFI in either model.

The HPV-stratified survival cohort included 216 HPV-negative and 23 HPV-positive patients, with 115 and eight OS events and 87 and seven PFI events, respectively. Schoenfeld residual-based tests did not identify statistically significant violations of the proportional hazards assumption, with global p-values of 0.60 for OS and 0.27 for PFI. The estimated association between *HEATR3* expression and OS was comparable between the non-stratified and HPV-stratified models. However, the small number of events among HPV-positive patients limits the interpretation of the stratified analyses. Furthermore, the stage I reference category included only 14 patients and three OS events, contributing to the wide confidence intervals observed for the stage IV versus stage I comparison.

Additional analyses were performed to assess the potential influence of cohort selection on the prognostic association of *HEATR3*. The initial survival population comprised 519 patients, including 220 OS events and 197 PFI events, with corresponding median follow-up times of 2.89 and 2.59 years. After restricting the population to patients with complete age, sex, and pathological stage information, 444 patients remained eligible for multivariable analysis. The further inclusion of anatomical tumor-site information reduced the analytical population to 239 patients, with 123 OS events and 94 PFI events and median follow-up times of 3.93 and 3.21 years, respectively.

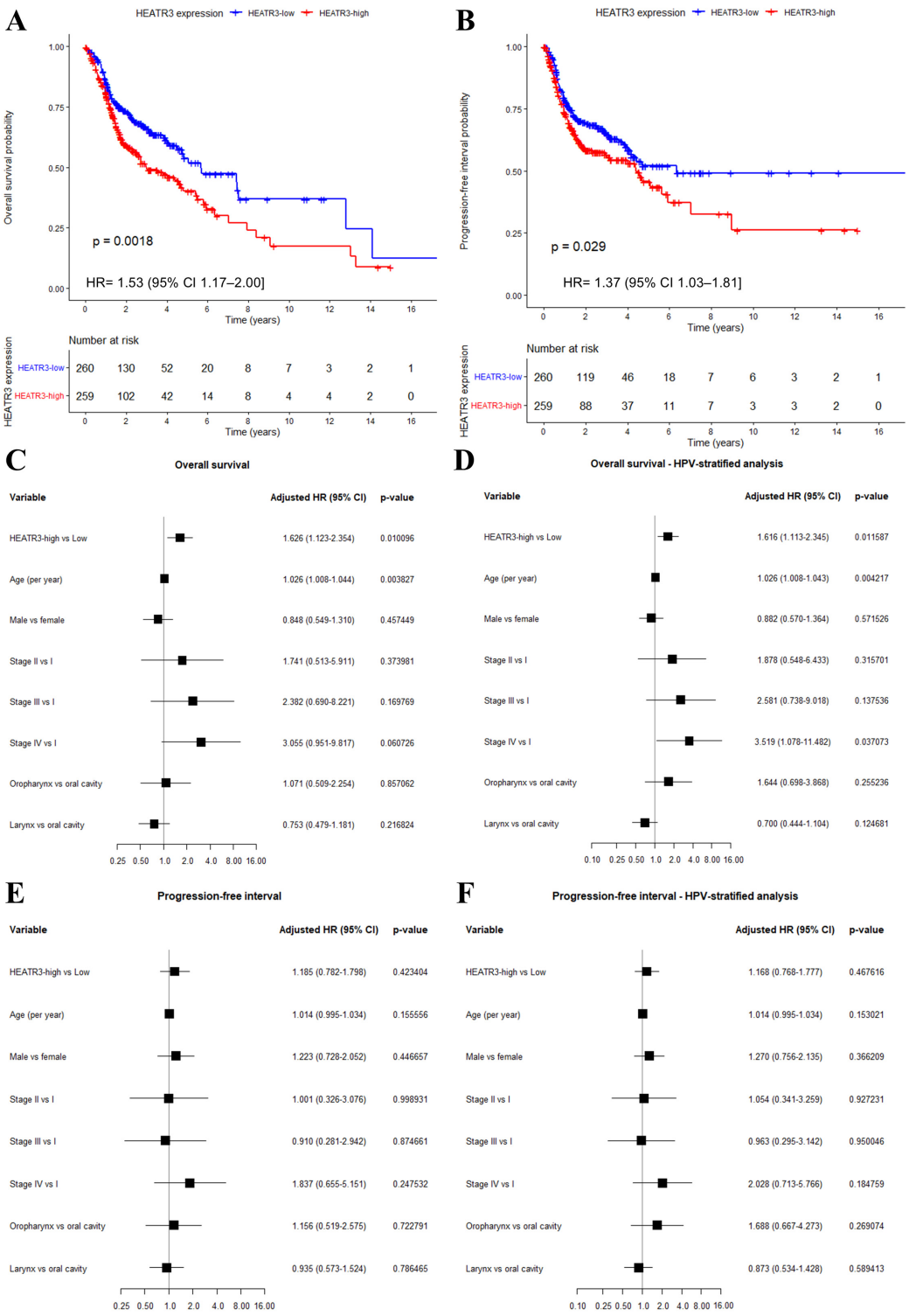


Figure 4. Prognostic significance of *HEATR3* expression in TCGA-HNSC patients. (**A**) Kaplan–Meier curves showing overall survival (OS) in patients with high and low *HEATR3* expression. (**B**) Kaplan–Meier curves showing progression-free interval (PFI) in the same expression groups. Patients were classified according to the median *HEATR3* expression level. (**C**) Forest plot of the multivariable Cox regression analysis for OS, adjusted for age, sex, clinical stage, and anatomical tumor site. (**D**) Forest plot of the HPV-stratified multivariable Cox regression analysis for OS. (**E**) Forest plot of the multivariable Cox regression analysis for PFI, adjusted for age, sex, clinical stage, and anatomical tumor site. (**F**) Forest plot of the HPV-stratified multivariable Cox regression analysis for PFI.

Comparisons between included and excluded patients revealed no statistically significant differences in age ($p = 0.19$), sex ($p = 0.71$), or pathological stage distribution among patients with available staging information ($p = 0.27$). However, anatomical-site distribution differed significantly among patients with available and eligible site annotations ($p = 4.61 \times 10^{-8}$). Sensitivity analyses showed that the association between high *HEATR3* expression and poorer OS remained statistically significant in the full cohort (unadjusted HR = 1.528, 95% CI: 1.168–1.999), the 444-patient cohort adjusted for age, sex, and stage (HR = 1.640, 95% CI: 1.222–2.200), and the corresponding model restricted to 239 patients (HR = 1.690, 95% CI: 1.175–2.431). Further adjustment for anatomical site yielded a comparable association (HR = 1.626, 95% CI: 1.123–2.354). These findings indicate relative stability of the *HEATR3*-associated OS estimates across the evaluated populations, although differences in anatomical-site composition and follow-up duration should be considered when interpreting the restricted cohort.

Thus, increased *HEATR3* expression is associated with poorer OS in TCGA-HNSC, after adjustment for the included clinicopathological covariates and stratification by HPV status. Conversely, the initial association with PFI was not retained following multivariable adjustment, suggesting that the prognostic association of *HEATR3* is more consistently supported for OS than for PFI.

3.5. Possible Associations of HEATR3 Expression with Cancer-Associated Fibroblasts and Endothelial Cells

To investigate the relationship between *HEATR3* expression and stromal components of the tumor microenvironment, tumor purity-adjusted Spearman correlation analyses were performed using multiple computational deconvolution algorithms implemented in TIMER3. The analyses focused on cancer-associated fibroblasts (CAFs) and endothelial cells in the overall TCGA-HNSC cohort (n = 520) and in HPV-positive (n = 97) and HPV-negative (n = 421) subgroups (Figure 5). In the overall TCGA-HNSC cohort, positive correlations with cancer-associated fibroblast (CAF) abundance were observed using TIDE ($\rho = 0.324$), EPIC ($\rho = 0.134$), and MCP-counter ($\rho = 0.127$), whereas xCell did not identify a significant association ($\rho = -0.082$). In HPV-positive tumors, TIDE revealed a positive correlation ($\rho = 0.381$), while xCell identified a significant inverse correlation ($\rho = -0.256$). In HPV-negative tumors, positive correlations were detected using TIDE ($\rho = 0.277$), EPIC ($\rho = 0.111$), and MCP-counter ($\rho = 0.106$). Associations with estimated endothelial-cell abundance were generally weaker and varied across algorithms. In the overall cohort, positive correlations were observed using MCP-counter ($\rho = 0.138$) and ConsensusTME ($\rho = 0.170$). Both algorithms also identified positive correlations in HPV-positive tumors ($\rho = 0.291$ and 0.232, respectively), whereas only ConsensusTME showed a significant association in HPV-negative tumors ($\rho = 0.123$).

These findings indicate that the associations between *HEATR3* expression and estimated stromal-cell abundance are modest and algorithm-dependent. Therefore, they should be considered exploratory and do not establish direct functional relationships between *HEATR3* and stromal-cell infiltration.



cancer	Cancer associated fibroblast EPIC	Cancer associated fibroblast MCP-COUNTER	Cancer associated fibroblast XCELL	Cancer associated fibroblast TIDE	Endothelial cell EPIC	Endothelial cell MCP-COUNTER	Endothelial cell XCELL	Endothelial cell CONSENSUS_TME
HNSC (n=520)	0.134	0.127	-0.082	0.324	0.015	0.138	0.011	0.17
HNSC-HPV+ (n=97)	0.117	0.067	-0.256	0.381	0.048	0.291	0.206	0.232
HNSC-HPV- (n=421)	0.111	0.106	-0.041	0.277	0.017	0.098	-0.055	0.123

Figure 5. Associations between *HEATR3* expression and computationally estimated cancer-associated fibroblast (CAF) and endothelial-cell abundance in the TCGA-HNSC cohort and HPV-defined subgroups. Correlations were obtained using TIMER3 with different cell abundance estimation algorithms. Heatmap values represent Spearman's rho (ϱ) correlation coefficients, with tumor purity adjustment applied through the TIMER3 correlation framework. Red and blue cells indicate statistically significant positive and negative correlations, respectively (nominal $p < 0.05$), whereas grey cells indicate non-significant associations. Differences between algorithms should be interpreted cautiously because cell abundance estimates are computationally inferred and method-dependent.

3.6. Functional Enrichment Analysis of HEATR3 Co-Expressed Genes in TCGA-HNSC

To investigate the biological processes and molecular pathways associated with *HEATR3* expression in TCGA-HNSC, the top 100 genes positively correlated with *HEATR3* in the TCGA-HNSC cohort were identified using GEPIA3. As shown in Figure 6A, GO enrichment analysis identified nine significantly enriched terms after Benjamini–Hochberg correction. The most significantly enriched biological processes (BP) were rRNA metabolic process, ribonucleoprotein complex biogenesis, ribosome biogenesis, and rRNA processing. Additional significant terms included maturation of SSU-rRNA, translational termination, and ribosomal large subunit biogenesis. Consistent with these findings, the cellular component (CC) analysis identified a significant enrichment of the preribosome component, whereas the molecular function (MF) analysis revealed significant enrichment of catalytic activity acting on RNA.

KEGG pathway enrichment analysis returned 152 pathways, none of which reached statistical significance after Benjamini–Hochberg correction (adjusted $p \geq 0.05$). The ten pathways with the lowest nominal *p*-values are displayed in Figure 6B for exploratory purposes only. Accordingly, no specific KEGG pathway enrichment was inferred from these results.

Overall, the functional enrichment analyses suggest that *HEATR3* expression in TCGA-HNSC is associated with transcriptional programs involved in RNA metabolism and ribosomal biogenesis. However, these findings are based on gene co-expression patterns and should be considered exploratory, without implying a direct regulatory role of *HEATR3* in these processes.

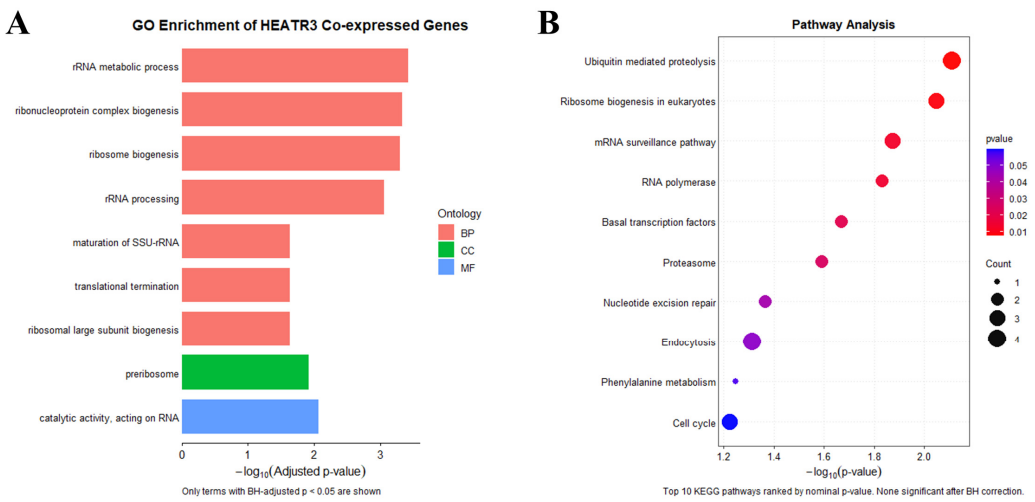


Figure 6. *HEATR3*-related gene enrichment analysis. (**A**) Gene Ontology (GO) enrichment analysis of the top 100 genes positively correlated with *HEATR3* expression in TCGA-HNSC, identified using GEPIA3. The bar plot shows significantly enriched terms (Benjamini–Hochberg-adjusted $p < 0.05$) across the three GO categories: Biological Process (BP, red), Cellular Component (CC, green), and Molecular Function (MF, blue). The horizontal axis represents −log10(adjusted *p*-value), with higher values indicating greater statistical significance. (**B**) KEGG analysis did not identify any pathways reaching statistical significance after multiple-testing correction and therefore did not provide additional evidence of functional enrichment. The bubble plot displays the 10 pathways with the lowest nominal *p*-values. The horizontal axis represents −log10(*p*-value), bubble size indicates the number of genes associated with each pathway, and bubble color reflects the corresponding nominal *p*-value. None of the identified KEGG pathways remained statistically significant after Benjamini–Hochberg correction (adjusted $p > 0.05$).

3.7. Protein Interaction Network and HEATR3–Protein Interaction Analysis

In order to further investigate the potential molecular interactions of *HEATR3* and its associated proteins, protein interaction network analyses were performed using STRING and BioGRID databases. As reported in Figure 7, STRING analysis of the top 100 *HEATR3* co-expressed genes revealed an interconnected protein association network comprising several functionally related protein groups (Figure 7A). A densely connected cluster included proteins involved in ribosome biogenesis and RNA processing, such as UTP4, UTP20, NIP7, TSR1, DDX18, DDX21, and NOC3L. Additional connections involved proteins associated with transcriptional regulation, RNA metabolism, and protein homeostasis, including POLR2C, TAF2, PSMD3, and PSMD7. *HEATR3* was positioned toward the periphery of the network, with connections to proteins associated with ribosomal maturation and RNA-related processes.

To extend this analysis, the BioGRID database was used to explore the broader interaction network associated with *HEATR3* (Figure 7B). The resulting network displayed a highly interconnected structure, with *HEATR3* occupying a central position and showing associations with numerous cellular proteins. Among the prominent nodes were PARK2, CUL3, CCNF, NPM1, EGFR, HNRNPA1, and several proteins involved in RNA processing, protein turnover, and cellular metabolism.

Overall, these analyses provided complementary views of the *HEATR3*-associated protein interaction landscape. While STRING highlighted functional associations predominantly related to ribosomal biogenesis and RNA metabolism, BioGRID revealed a broader network encompassing proteins involved in multiple cellular processes. These findings suggest that *HEATR3* may be associated with complex molecular networks relevant to cellular homeostasis, although the functional significance of individual

interactions and their potential involvement in HNSCC biology require further experimental investigation.

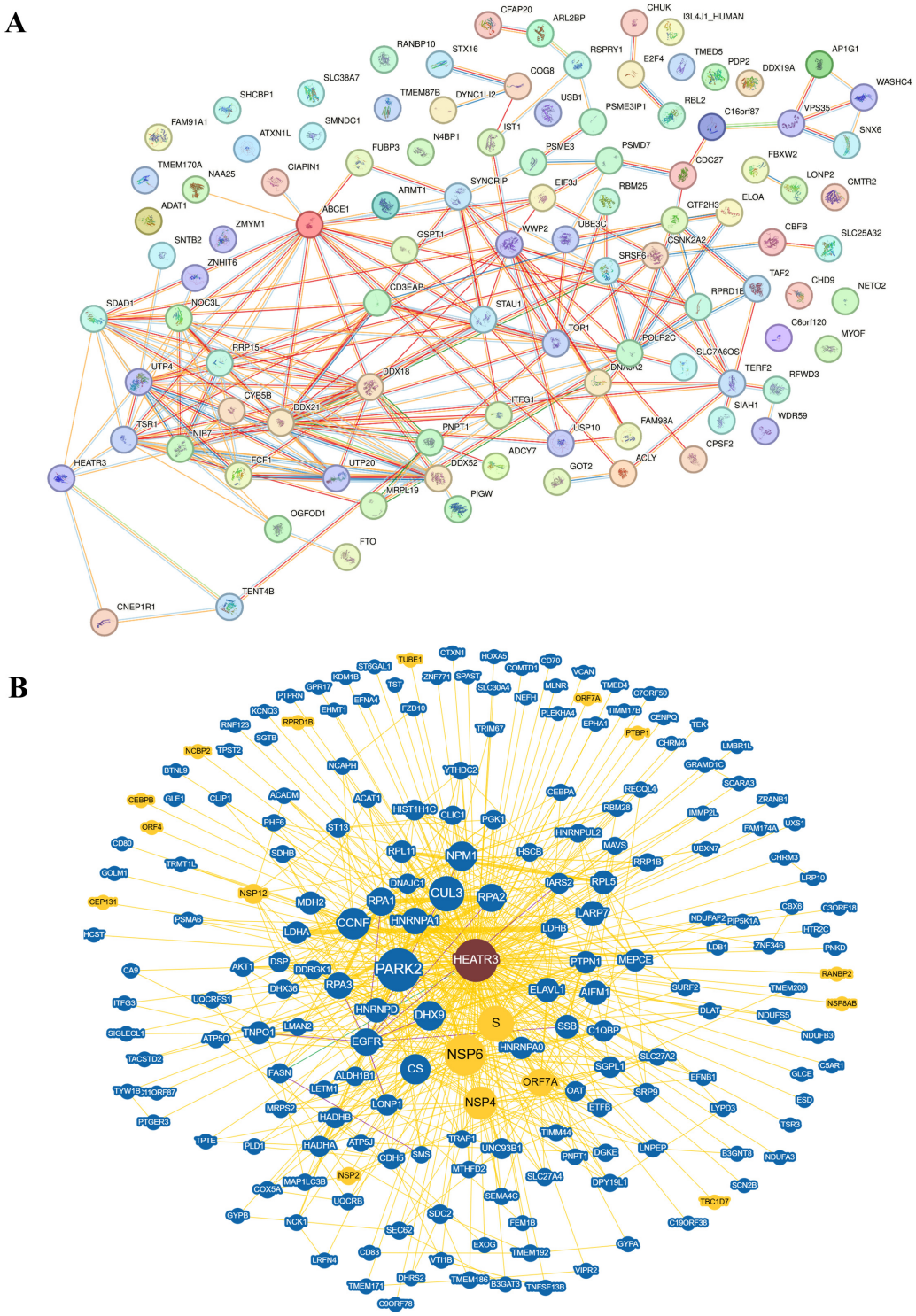


Figure 7. Protein interaction network analysis of *HEATR3* and associated proteins. (**A**) Protein–protein association network of *HEATR3* and its co-expressed genes in TCGA-HNSC, generated using the STRING database. (**B**) *HEATR3* protein interactions obtained from BioGRID.

3.8. Correlation Analysis of HEATR3 with Genes Associated with TCGA-HNSC/OSCC Progression

An exploratory post hoc analysis identified positive correlations between *HEATR3* and six genes (*ACLY*, *CIAPIN1*, *E2F4*, *FTO*, *SHCBP1*, and *SRSF6*) previously associated with molecular processes relevant to HNSCC or OSCC (Figure 8) [32–37]. The strongest associations were observed for *CIAPIN1* (r = 0.70, $p = 2.6 \times 10^{-78}$) and *E2F4* (r = 0.68, $p = 1.1 \times 10^{-72}$), followed by *SHCBP1* (r = 0.62, $p = 9.3 \times 10^{-57}$), *FTO* (r = 0.61, $p = 1.7 \times 10^{-54}$), *SRSF6* (r = 0.60, $p = 3.6 \times 10^{-52}$), and *ACLY* (r = 0.58, $p = 1.2 \times 10^{-48}$). These genes were selected based on their reported biological relevance rather than a predefined selection criterion. Given the post hoc selection and the absence of multiple-testing correction, these associations were considered descriptive and were not interpreted as evidence of a specific progression-related molecular signature. The differences among the correlation coefficients were not formally tested, and the reproducibility of these associations requires evaluation in independent datasets.

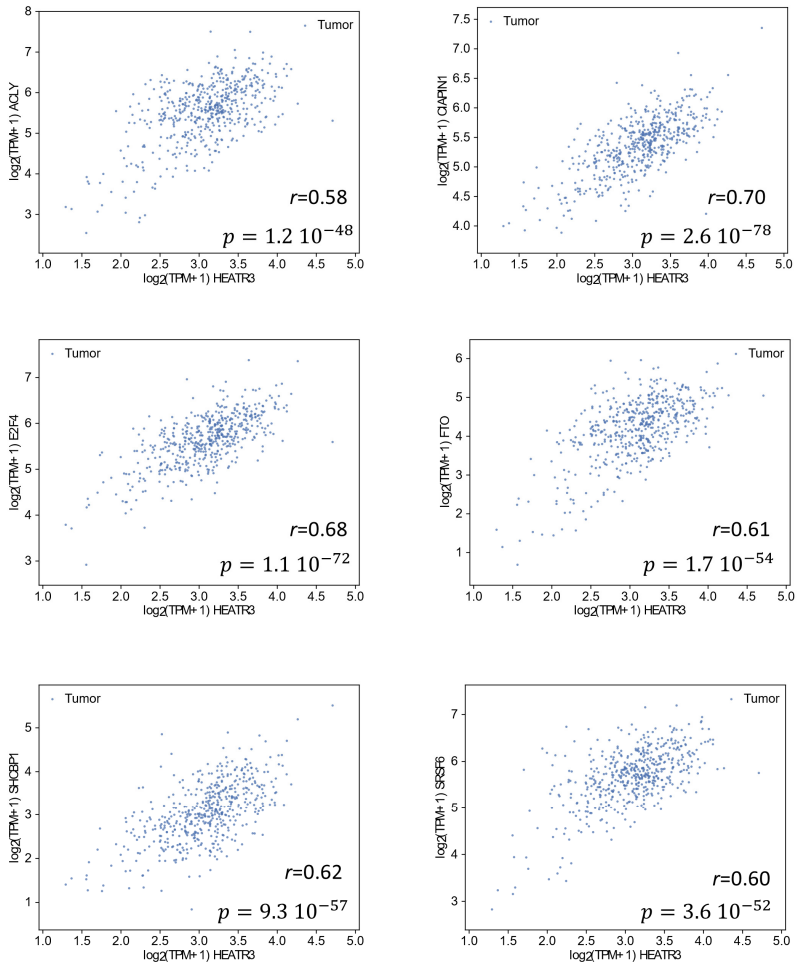


Figure 8. Correlation analysis between *HEATR3* and *ACLY*, *CIAPIN1*, *E2F4*, *FTO*, *SHCBP1*, and *SRSF6* in TCGA-HNSC cancer samples. Scatter plots show the relationship between *HEATR3* expression and *ATP citrate lyase (ACLY)*, *Cytokine-induced apoptosis inhibitor 1 (CIAPIN1)*, *E2F transcription factor 4 (E2F4)*, *FTO alpha-ketoglutarate-dependent dioxygenase (FTO)*, *SHC binding and spindle associated 1 (SHCBP1)* and *Serine and arginine rich splicing factor 6 (SRSF6)* expression in TCGA-HNSC tumor samples, as determined using GEPIA3. Each point represents an individual tumor sample. *HEATR3* and target-gene expression values are reported as log2(TPM + 1). Pearson's correlation coefficient (r) and the corresponding *p*-value are reported in each panel. Each coefficient describes the association between *HEATR3* and a different gene; differences among coefficients were not formally evaluated.

3.9. Validation of HEATR3 Expression in Two Independent Cohorts

In order to validate the results regarding *HEATR3* expression in TCGA-HNSC, we analyzed *HEATR3* expression in two independent OSCC cohorts: GSE37991 and GSE30784. The main characteristics of these datasets are summarized in Table 1.

Analysis of GSE37991, comprising 40 paired OSCC and non-tumor oral epithelial samples, revealed significantly higher *HEATR3* expression in tumor tissues compared to normal tissues (Figure 9A). Using the ILMN_1808219 probe, *HEATR3* exhibited a log2 fold change (log2FC) of 0.285 (95% CI: 0.177–0.393; BH-adjusted $p = 1.97 \times 10^{-5}$). The paired expression analysis and corresponding heatmap further illustrated the increased *HEATR3* expression in OSCC specimens (Figure 9A). Consistent results were obtained with the alternative *HEATR3* probe, ILMN_1666082, which also showed significant upregulation in tumor tissues (log2FC = 0.289; BH-adjusted $p = 6.16 \times 10^{-7}$).

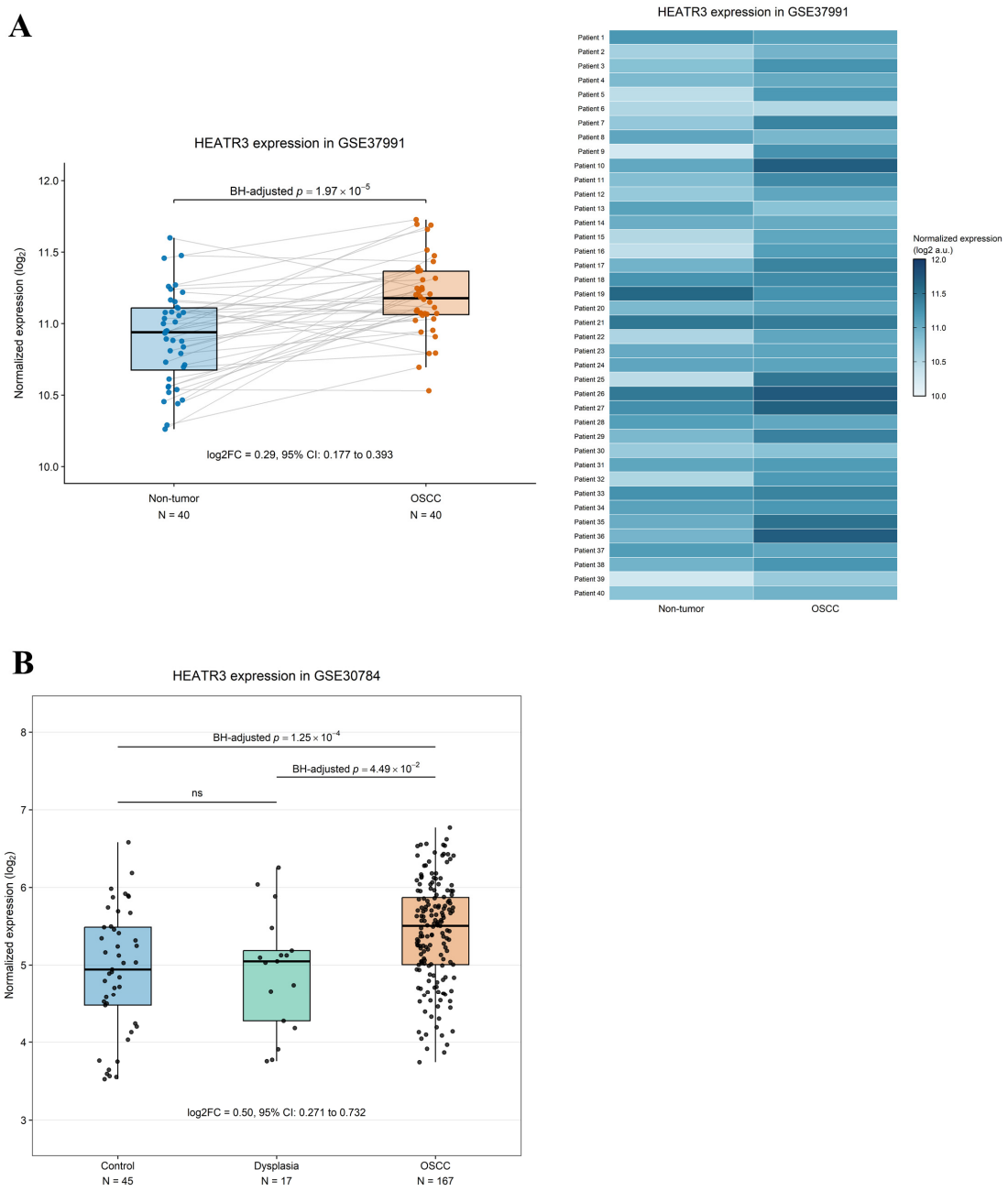


Figure 9. Independent validation of *HEATR3* expression in two OSCC cohorts. (**A**) *HEATR3* expression in the GSE37991 cohort, comprising paired OSCC samples (N = 40, orange) and adjacent non-tumor tissues (N = 40, blue) from the same patients. Expression values were quantile-normalized

and log2-transformed. In the boxplot, grey lines connect paired samples from the same patient. The adjacent heatmap shows *HEATR3* expression for each matched patient pair, with increasing color intensity indicating higher expression. (**B**) *HEATR3* expression in the independent GSE30784 cohort comprising normal oral tissues (N = 45; blue), oral dysplasia samples (N = 17; green), and OSCC samples (N = 167; orange). CI, confidence interval; BH, Benjamini–Hochberg; ns, not significant.

HEATR3 expression was subsequently evaluated in GSE30784, which included 45 normal controls, 17 oral dysplasia samples, and 167 OSCC specimens (Figure 9B). Analysis using the 1554478_a_at probe demonstrated significantly increased *HEATR3* expression in OSCC compared with normal controls (log2FC = 0.502; 95% CI: 0.271–0.732; BH-adjusted $p = 1.25 \times 10^{-4}$). *HEATR3* expression was also significantly higher in OSCC than in oral dysplasia samples (log2FC = 0.503; 95% CI: 0.154–0.853; BH-adjusted $p = 0.0449$), whereas no significant difference was observed between dysplastic and normal tissues (BH-adjusted $p = 0.999$) (Figure 9B). In contrast, the alternative *HEATR3* probe, 219289_at, did not reveal significant expression differences among the three groups.

Overall, these analyses identified increased *HEATR3* expression in OSCC specimens across two independent GEO datasets, with consistent results for both probes in GSE37991 and a significant increase detected by one of the two probes in GSE30784. These findings provide additional transcriptomic evidence supporting the association between elevated *HEATR3* expression and OSCC.

4. Discussion

HEATR3 is a HEAT repeat-containing protein involved in ribosomal protein trafficking and ribosome assembly. Previous experimental studies have demonstrated its contribution to the nuclear import of the ribosomal protein RPL5 and to the maintenance of ribosomal homeostasis [25]. *HEATR3* has also been implicated in nucleolar surveillance mechanisms associated with p53 stabilization following disturbances in ribosome biogenesis [24]. These established molecular functions provide a relevant biological context for investigating *HEATR3* in malignancies characterized by alterations in cellular growth and protein synthesis. In our analysis, *HEATR3* was broadly expressed across normal human tissues and cellular populations, including squamous epithelial cells and several immune cell populations indicating that *HEATR3* is not restricted to malignant tissues. We also found that *HEATR3* expression was significantly increased in TCGA-HNSC tissues compared with non-cancerous controls suggesting an association between increased *HEATR3* expression and TCGA-HNSC. In addition, *HEATR3* expression did not differ significantly across TCGA-HNSC pathological stages I–IV suggesting that the higher expression detected in TCGA-HNSC tissues is not accompanied by a clear stage-dependent increase within the analyzed cohort. Importantly, the observed increase in *HEATR3* expression was not investigated exclusively in metastatic tumors, as the TCGA-HNSC cohort included patients with different pathological stages. However, pathological stage does not directly indicate metastatic status, and separate analyses according to lymph node involvement or distant metastasis were not performed. Therefore, the present findings do not establish a specific association between *HEATR3* expression and metastatic disease.

The genomic characterization of *HEATR3* provided an additional perspective. Alterations affecting this gene were detected in approximately 1% of TCGA-HNSC cases and consisted mainly of amplifications and somatic mutations. No *HEATR3* mutations were identified in the smaller MD Anderson OSCC cohort, although this finding should be interpreted cautiously because of the limited sample size. The two identified missense variants in TCGA-HNSC were classified as variants of uncertain significance. Given the low frequency of these alterations, recurrent somatic mutations and high-level gene amplifications are unlikely to represent major mechanisms underlying the increased *HEATR3*

expression observed in TCGA-HNSC. Alternative mechanisms may involve epigenetic regulation, changes in promoter or enhancer activity, altered transcription factor activity, or post-transcriptional regulation of mRNA stability. However, these possibilities remain hypothetical, as the present study did not investigate *HEATR3* promoter methylation, chromatin modifications, transcriptional regulation, or mRNA turnover. Further studies are therefore needed to identify the mechanisms responsible for increased *HEATR3* expression in HNSCC.

One of the main findings of this study was the association between *HEATR3* expression and patient survival. In TCGA-HNSC, patients with high *HEATR3* expression exhibited significantly poorer OS than those with low expression, as shown by the Kaplan–Meier survival curves (Figure 4A). This association persisted after adjustment for age, sex, pathological stage, and anatomical tumor site in the multivariable Cox regression analysis (Figure 4C). A comparable association was observed in the HPV-stratified multivariable model. These findings indicate that the association between *HEATR3* expression and OS is not fully explained by the clinicopathological covariates included in the models. However, the present analyses do not establish whether *HEATR3* provides incremental prognostic value beyond established clinical predictors, as improvements in model discrimination, calibration, and clinical utility were not evaluated. However, the relationship with progression-free interval (PFI) was less consistent. Although high *HEATR3* expression was associated with shorter PFI in the unadjusted analysis, this association was not statistically significant after multivariable adjustment. The absence of significant differences in *HEATR3* expression across pathological stages does not contradict its association with overall survival after multivariable adjustment. These analyses address distinct aspects of tumor biology, as stage-related expression differences are not necessarily required for a molecular marker to be associated with patient prognosis. However, the present findings do not establish whether *HEATR3* provides additional clinical predictive value beyond established prognostic factors. Furthermore, the loss of statistical significance for PFI after adjustment should be interpreted cautiously, considering the reduced number of events and the uncertainty reflected by the confidence interval. Thus, the prognostic relevance of *HEATR3* in the present dataset is more consistently supported for OS than for PFI.

Tumor microenvironment analyses revealed modest and algorithm-dependent associations between *HEATR3* expression and estimated stromal-cell abundance. The discrepancies observed across TIDE, EPIC, xCell, MCP-counter, and ConsensusTME may reflect differences in reference gene signatures, computational approaches, and the way individual algorithms estimate cell abundance. Notably, the opposite correlations identified by TIDE and xCell for CAFs in HPV-positive tumors indicate that these associations are not consistently reproduced across methods. Moreover, estimates derived from bulk transcriptomic data do not directly measure cellular infiltration and may be influenced by tumor heterogeneity and differences in cell-type transcriptional profiles. Therefore, these findings remain exploratory and cannot establish a functional role for *HEATR3* in regulating the tumor microenvironment.

Functional enrichment analyses offered additional insight into the molecular context associated with *HEATR3* expression. Gene Ontology analysis of *HEATR3*-correlated genes identified significant enrichment of biological processes involving rRNA metabolism, ribonucleoprotein complex biogenesis, ribosome biogenesis, and rRNA processing. Significant associations were also observed for the preribosome cellular component and catalytic activity acting on RNA. These findings are consistent with the established involvement of *HEATR3* in ribosomal homeostasis and suggest that its expression is associated with transcriptional programs related to RNA processing and ribosomal assembly in TCGA-HNSC. STRING and BioGRID analyses provided complementary information on *HEATR3*-associated molecular networks. STRING highlighted functional associations

involving proteins related to ribosome biogenesis and RNA metabolism, whereas BioGRID identified a broader set of experimentally reported interactions. However, STRING associations may arise from multiple evidence sources, including co-expression, curated databases, and literature-based information, and do not necessarily indicate direct physical binding. Similarly, BioGRID interactions may reflect indirect associations identified through different experimental approaches and biological systems. Accordingly, these network analyses should be regarded as exploratory and cannot establish direct molecular interactions or their functional relevance in HNSCC cells. In contrast, KEGG analysis did not identify any pathways reaching statistical significance after multiple-testing correction and therefore did not provide additional evidence of functional enrichment.

Exploratory analyses also identified positive correlations between *HEATR3* and selected genes previously implicated in TCGA-HNSC or OSCC-related molecular processes including *ACLY*, *CIAPIN1*, *E2F4*, *FTO*, *SHCBP1*, and *SRSF6* [32–37]. However, these genes were selected post hoc, and the observed correlations do not establish functional relationships or provide independent evidence of *HEATR3* involvement in tumor progression. Therefore, these findings should be considered descriptive and hypothesis-generating.

An important component of the present study was the independent validation of *HEATR3* expression in OSCC. In the GSE37991 cohort, comprising 40 matched pairs of tumor and non-tumor oral epithelial samples, *HEATR3* expression was significantly higher in OSCC specimens. Similar results were found in the GSE30784 cohort, which included 45 normal controls, 17 oral dysplasia samples, and 167 OSCC specimens, where *HEATR3* expression was significantly higher in OSCC than in normal controls and dysplastic tissues. No significant difference was detected between dysplastic and normal samples using this probe. However, these findings require cautious interpretation. In GSE37991, the increase in *HEATR3* expression was relatively modest, corresponding to approximately 22% on the original expression scale, although statistically significant and consistent across both probes. In contrast, the results obtained in GSE30784 were probe-dependent, as the alternative probe, 219289_at, did not show significant expression differences among the analyzed groups. Such discrepancies may arise from differences in probe specificity, transcript regions targeted, hybridization characteristics, or annotation accuracy. However, these potential explanations were not directly investigated. Consequently, the independent transcriptomic analyses provide supporting, but not uniformly concordant, evidence of increased *HEATR3* expression in OSCC. Moreover, these independent cohorts were used exclusively for expression validation, as survival endpoints were not available for the corresponding prognostic analyses. Consequently, the association between *HEATR3* expression and patient survival remains supported by TCGA-HNSC alone and requires confirmation in independent cohorts with adequate clinical follow-up.

Overall, the results establish a consistent association between *HEATR3* expression and several molecular and clinical characteristics of TCGA-HNSC. The relationship with OS represents the most relevant clinical observation, whereas the enrichment of ribosome-associated processes provides a biological context consistent with the known functions of *HEATR3*. Independent expression analyses in OSCC further extend these observations to a specific anatomical subset of HNSCC. These findings support continued investigation of *HEATR3* as a candidate molecular biomarker, particularly in relation to patient prognosis.

5. Limitations

Although this study provided evidence regarding *HEATR3* expression in TCGA-HNSC and OSCC, several limitations should be acknowledged. First, this study was based on retrospective analyses of publicly available datasets, with differences in patient characteristics, anatomical sites, and analytical platforms. The availability of anatomical

tumor-site annotations restricted the more detailed multivariable survival analyses to 239 patients. Although sensitivity analyses showed relatively stable *HEATR3*-associated OS estimates across different analytical populations, significant differences in anatomical-site composition and follow-up duration were observed. Therefore, potential selection bias cannot be excluded, and the prognostic findings require validation in independent cohorts with more complete clinical annotations. Second, the HPV-stratified Cox models included only 23 HPV-positive patients, with eight OS events and seven PFI events, limiting the precision of these analyses. In addition, HPV classifications used for survival and tumor microenvironment analyses were obtained from different annotation sources and analytical populations. Although the association between *HEATR3* expression and OS remained stable following HPV stratification, these findings should be interpreted as supplementary evidence rather than independent prognostic validation within HPV-defined subgroups. In addition, the use of the median *HEATR3* expression level as a cutoff may have reduced statistical power and does not provide a clinically validated threshold. In addition, although the number of events was generally adequate relative to the total number of model coefficients, estimates involving sparsely represented categories remained imprecise. The reduced number of PFI events in the fully adjusted models may also have limited the ability to detect an association. Third, functional enrichment, protein interaction, and tumor microenvironment analyses were primarily based on computational associations and did not establish direct biological mechanisms. Finally, experimental validation, whether by immunohistochemistry, quantitative PCR, or perturbation in cell lines, is necessary to assess *HEATR3* cellular and subcellular localization. Thus, additional clinical validation and experimental investigations, including assessment of *HEATR3* protein expression, would help further characterize its prognostic and biological relevance in HNSCC.

6. Conclusions

The present study identified increased *HEATR3* expression in TCGA-HNSC patients and demonstrated a significant association between elevated *HEATR3* transcript levels and poorer overall survival in TCGA-HNSC patients. This prognostic association persisted after adjustment for relevant clinicopathological variables and HPV stratification. Functional enrichment and protein interaction analyses further associated *HEATR3* with molecular networks involved in ribosome biogenesis and RNA metabolism, consistent with its established biological functions. Independent analyses of two OSCC datasets provided additional evidence of increased *HEATR3* expression in malignant oral tissues. Collectively, these findings support *HEATR3* as a candidate prognostic biomarker in HNSCC. Further studies should validate its association with survival in independent patient cohorts, determine whether it improves prognostic performance beyond established clinicopathological variables, and assess HEATR3 protein expression and its potential functional involvement in tumor biology.

Supplementary Materials: The following supporting information can be downloaded at https://www.mdpi.com/article/10.3390/genes17111462/s1: Table S1: GO and KEGG results; Table S2: Top 100 *HEATR3*-related genes.

Author Contributions: Conceptualization, G.T. and R.C.; methodology, G.T. and R.C.; software, R.C.; validation, G.T., M.S. and R.C.; formal analysis, G.T. and R.C.; investigation, G.T., M.S. and R.C.; resources, G.T.; data curation, G.T. and R.C.; writing—original draft preparation, G.T. and R.C.; writing—review and editing, G.T., M.S. and R.C.; visualization, G.T. and R.C.; supervision, G.T. and R.C.; project administration, G.T. and R.C. All authors have read and agreed to the published version of the manuscript.

https://doi.org/10.3390/genes17111462

Funding: This research received no external funding.

Institutional Review Board Statement: Not applicable.

Informed Consent Statement: Not applicable.

Data Availability Statement: The publicly available datasets analyzed in this study were obtained from The Cancer Genome Atlas (TCGA-HNSC) and the Gene Expression Omnibus (GEO; accession numbers GSE30784 and GSE37991). To ensure transparency and facilitate independent reproducibility, the R script used for the bioinformatic and statistical analyses, together with the corresponding input tables and supporting files, has been provided as Supplementary Materials.

Conflicts of Interest: The authors declare no conflicts of interest.

Abbreviations

The following abbreviations are used in this manuscript:

ATP	Adenosine Triphosphate
BH	Benjamini–Hochberg
ConsensusTME	Consensus Tumor Microenvironment Estimation
EPIC	Estimating the Proportions of Immune and Cancer Cells
GEO	Gene Expression Omnibus
GEPIA3	Gene Expression Profiling Interactive Analysis, version 3
GO	Gene Ontology
HEAT	Huntingtin, Elongation Factor 3, Protein Phosphatase 2A, and TOR1
HEATR3	HEAT Repeat-Containing Protein 3
HNSC	Head and Neck Squamous Cell Carcinoma (TCGA dataset designation)
HNSCC	Head and Neck Squamous Cell Carcinoma
HPV	Human Papillomavirus
KEGG	Kyoto Encyclopedia of Genes and Genomes
log2FC	Log2 Fold Change
MCP-counter	Microenvironment Cell Populations-counter
OS	Overall Survival
OSCC	Oral Squamous Cell Carcinoma
PFI	Progression-Free Interval
SSU-rRNA	Small Subunit Ribosomal RNA
STRING	Search Tool for the Retrieval of Interacting Genes/Proteins
TCGA	The Cancer Genome Atlas
TIDE	Tumor Immune Dysfunction and Exclusion
TIMER3	Tumor Immune Estimation Resource, version 3
TPM	Transcripts per Million
xCell	Cell-type Enrichment and Estimation Method

References

1. Dunn, L.A.; Ho, A.L.; Pfister, D.G. Head and Neck Cancer: A Review. *JAMA* **2026**, *335*, 531–541. https://doi.org/10.1001/jama.2025.21733.
2. Johnson, D.E.; Burtness, B.; Leemans, C.R.; Lui, V.W.Y.; Bauman, J.E.; Grandis, J.R. Head and neck squamous cell carcinoma. *Nat. Rev. Dis. Primers* **2020**, *6*, 92. https://doi.org/10.1038/s41572-020-00224-3.
3. Bray, F.; Laversanne, M.; Sung, H.; Ferlay, J.; Siegel, R.L.; Soerjomataram, I.; Jemal, A. Global cancer statistics 2022: GLOBOCAN estimates of incidence and mortality worldwide for 36 cancers in 185 countries. *CA Cancer J. Clin.* **2024**, *74*, 229–263. https://doi.org/10.3322/caac.21834.
4. Goncalves, M.W.A.; de Lima-Souza, R.A.; Ribeiro-de-Assis, M.C.F.; Cattan, M.E.S.; Egal, E.S.A.; Altemani, A.; Mariano, F.V. Prognostic implications across histological subtypes of head and neck squamous cell carcinoma: An update. *J. Stomatol. Oral. Maxillofac. Surg.* **2025**, *126*, 102149. https://doi.org/10.1016/j.jormas.2024.102149.
5. Park, E.; Kang, H.Y.; Jung, Y.S.; Kim, B.; Bui, T.T.; Oh, J.K. Smoking, Alcohol, and Their Interaction in the Risk of Head and Neck Cancer: A Nationwide Cohort Study. *Cancer Med.* **2026**, *15*, e71665. https://doi.org/10.1002/cam4.71665.
6. Golusinski, W.; Golusinska-Kardach, E.; Machczynski, P.; Szewczyk, M. HPV-Driven Head and Neck Cancer: The European Perspective. *Viruses* **2025**, *17*, 662. https://doi.org/10.3390/v17050662.
7. Yuan, Y.; Huang, J.W.; Cao, J.L.; Wu, J.H.; Wang, L.L.; Gan, H.; Xu, J.H.; Ye, F. Tobacco and alcohol use are the risk factors responsible for the greatest burden of head and neck cancers: A study from the Global Burden of Disease Study 2019. *Ann. Med.* **2025**, *57*, 2500693. https://doi.org/10.1080/07853890.2025.2500693.
8. Quiroga-Garza, J.M.; Herrera-Saldivar, M.F.; Hernandez-Bautista, N.C.; Alanis-Valdez, A.Y.; Flores-Flores, A.S.; Vazquez-Guillen, J.M.; Resendez-Perez, D.; Tamez-Guerra, R.S.; Rodriguez-Padilla, C. Oncogenic viruses and their role in oral cavity and oropharyngeal squamous cell carcinoma: A systematic review. *Front. Oncol.* **2026**, *16*, 1806640. https://doi.org/10.3389/fonc.2026.1806640.
9. Togni, L.; Mascitti, M.; Sartini, D.; Campagna, R.; Pozzi, V.; Salvolini, E.; Offidani, A.; Santarelli, A.; Emanuelli, M. Nicotinamide N-Methyltransferase in Head and Neck Tumors: A Comprehensive Review. *Biomolecules* **2021**, *11*, 1594. https://doi.org/10.3390/biom11111594.
10. Khodadadi, M.; Khodadadi, M. Malignant transformation rate of oral precancerous disorders to oral cancer: Systematic review and meta-analysis of the current evidence. *Front. Oral. Health* **2025**, *6*, 1673474. https://doi.org/10.3389/froh.2025.1673474.
11. Jovanova, E.; Angjelova, A.; Campagna, R.; Polizzi, A.; Marya, A.; Isola, G. From Inflamed Gingiva to Invasive Malignancy: Molecular Crosstalk in Oral Carcinogenesis: A Scoping Review. *Front. Biosci.* **2026**, *31*, 53502. https://doi.org/10.31083/FBL53502.
12. Yasothkumar, D.; Ramani, P.; Ramasubramanian, A. Clinico-Pathological Assessment and Malignant Transformation in Patients with Oral Epithelial Dysplasia—A Follow-up Cohort Study. *Head Neck Pathol.* **2025**, *19*, 96. https://doi.org/10.1007/s12105-025-01833-8.
13. Fang, Y.; Yi, C.; Sun, R.; Shen, B.; Yao, M.; Yang, Y.; Ni, Y.; Liu, Y.; Li, Z.; Liu, J. Global Annualized Recurrence Rates and Dynamic Risk Profiles in Head and Neck Cancer. *Int. J. Cancer* **2026**, *160*, 44–56. https://doi.org/10.1002/ijc.70675.
14. Polizzi, A.; Isola, G.; Cecati, M.; Bonci, N.; Campagna, R.; Tossetta, G. Resveratrol in Oral Squamous Cell Carcinoma: Preclinical Evidence and Translational Opportunities. *Oncol. Res.* **2026**, *34*, 10. https://doi.org/10.32604/or.2026.079642.
15. Saini, K.S.; Somara, S.; Ko, H.C.; Thatai, P.; Quintana, A.; Wallen, Z.D.; Green, M.F.; Mehrotra, R.; McGuigan, S.; Pang, L.; et al. Biomarkers in head and neck squamous cell carcinoma: Unraveling the path to precision immunotherapy. *Front. Oncol.* **2024**, *14*, 1473706. https://doi.org/10.3389/fonc.2024.1473706.
16. Schiavoni, V.; Emanuelli, M.; Sartini, D.; Salvolini, E.; Pozzi, V.; Campagna, R. Curcumin and its Analogues in Oral Squamous Cell Carcinoma: State-of-the-art and Therapeutic Potential. *Anticancer Agents Med. Chem.* **2025**, *25*, 313–329. https://doi.org/10.2174/0118715206297840240510063330.
17. Gitareja, K.; Chelliah, S.S.; Sanij, E.; Sandhu, S.; Kang, J.; Khot, A. Ribosome Biogenesis and Function in Cancer: From Mechanisms to Therapy. *Cancers* **2025**, *17*, 2534. https://doi.org/10.3390/cancers17152534.
18. Fan, W.; Liu, H.; Yang, L.; Sinha, N.; Catipovic, M.; Dong, D.; Easawaran, H.; Green, R.; Laiho, M. mTOR inactivation governs adaptive survival to ribosome biogenesis deficiency. *Genes. Dev.* **2026**, *40*, 1855–1870. https://doi.org/10.1101/gad.353708.126.
19. Lawrence, I.R.; Sutton, E.C.; Bhaskar, S.; Baserga, S.J. Signaling to make human ribosomes: Connections between the cytoplasm and the nucleolus. *Mol. Cell* **2026**, *86*, 469–490. https://doi.org/10.1016/j.molcel.2026.01.007.
20. Hwang, S.P.; Denicourt, C. The impact of ribosome biogenesis in cancer: From proliferation to metastasis. *NAR Cancer* **2024**, *6*, zcae017. https://doi.org/10.1093/narcan/zcae017.

21. Cerezo, E.L.; Henry, Y.; Henras, A.K.; Romeo, Y. Ribosome biogenesis and homeostasis: In the front line to cope with cellular stress. *Biochimie* **2025**, *238*, 43–56. https://doi.org/10.1016/j.biochi.2025.08.016.
22. Howard, G.C.; Tansey, W.P. Ribosome-directed cancer therapies: The tip of the iceberg? *Trends Pharmacol. Sci.* **2025**, *46*, 303–310. https://doi.org/10.1016/j.tips.2025.02.001.
23. Delfino, O.; Xuan, J.; Hein, N.; Ferreira, R.; Hannan, R.D.; George, A.J. The Nucleolus in Human Disease: Ribosome Biogenesis, Nucleolar Surveillance, and Therapeutic Opportunities. *Biomolecules* **2026**, *16*, 1121. https://doi.org/10.3390/biom16081121.
24. Hannan, K.M.; Soo, P.; Wong, M.S.; Lee, J.K.; Hein, N.; Poh, P.; Wysoke, K.D.; Williams, T.D.; Montellese, C.; Smith, L.K.; et al. Nuclear stabilization of p53 requires a functional nucleolar surveillance pathway. *Cell Rep.* **2022**, *41*, 111571. https://doi.org/10.1016/j.celrep.2022.111571.
25. O'Donohue, M.F.; Da Costa, L.; Lezzerini, M.; Unal, S.; Joret, C.; Bartels, M.; Brilstra, E.; Scheijde-Vermeulen, M.; Wacheul, L.; De Keersmaecker, K.; et al. *HEATR3* variants impair nuclear import of uL18 (RPL5) and drive Diamond-Blackfan anemia. *Blood* **2022**, *139*, 3111–3126. https://doi.org/10.1182/blood.2021011846.
26. Nakamura, A.; Kakihara, Y.; Funayama, A.; Haga, K.; Mikami, T.; Kobayashi, D.; Yoshida, Y.; Izumi, K.; Kobayashi, T.; Saeki, M. HEATR1, a novel interactor of Pontin/Reptin, stabilizes Pontin/Reptin and promotes cell proliferation of oral squamous cell carcinoma. *Biochem. Biophys. Res. Commun.* **2021**, *557*, 294–301. https://doi.org/10.1016/j.bbrc.2021.04.021.
27. Yang, X.M.; Wang, X.Q.; Hu, L.P.; Feng, M.X.; Zhou, Y.Q.; Li, D.X.; Li, J.; Miao, X.C.; Zhang, Y.L.; Yao, L.L.; et al. Nucleolar HEAT Repeat Containing 1 Up-regulated by the Mechanistic Target of Rapamycin Complex 1 Signaling Promotes Hepatocellular Carcinoma Growth by Dominating Ribosome Biogenesis and Proteome Homeostasis. *Gastroenterology* **2023**, *165*, 629–646. https://doi.org/10.1053/j.gastro.2023.05.029.
28. Haesen, D.; Abbasi Asbagh, L.; Derua, R.; Hubert, A.; Schrauwen, S.; Hoorne, Y.; Amant, F.; Waelkens, E.; Sablina, A.; Janssens, V. Recurrent *PPP2R1A* Mutations in Uterine Cancer Act through a Dominant-Negative Mechanism to Promote Malignant Cell Growth. *Cancer Res.* **2016**, *76*, 5719–5731. https://doi.org/10.1158/0008-5472.CAN-15-3342.
29. Kang, Y.J.; Pan, L.; Liu, Y.; Rong, Z.; Liu, J.; Liu, F. GEPIA3: Enhanced drug sensitivity and interaction network analysis for cancer research. *Nucleic Acids Res.* **2025**, *53*, W283–W290. https://doi.org/10.1093/nar/gkaf423.
30. Rotondo, R.; Polizzi, A.; Zeppa, S.D.; Isola, G.; Campagna, R.; Tossetta, G. Transcriptomic Profiling Reveals METTL26 as a Potential Biomarker in Head and Neck Squamous Cell Carcinoma with Independent Validation in Oral Squamous Cell Carcinoma. *Med. Sci.* **2026**, *14*, 674. https://doi.org/10.3390/medsci14060674.
31. Liu, J.; Lichtenberg, T.; Hoadley, K.A.; Poisson, L.M.; Lazar, A.J.; Cherniack, A.D.; Kovatich, A.J.; Benz, C.C.; Levine, D.A.; Lee, A.V.; et al. An Integrated TCGA Pan-Cancer Clinical Data Resource to Drive High-Quality Survival Outcome Analytics. *Cell* **2018**, *173*, 400–416 e411. https://doi.org/10.1016/j.cell.2018.02.052.
32. Yan, L.; Wang, J.; Li, B.; Guo, J.; Jia, R. The splicing factor SRSF6 mediates ferroptosis resistance in head and neck squamous cell carcinoma through induction of stearoyl-CoA desaturase. *J. Biol. Chem.* **2025**, *301*, 110509. https://doi.org/10.1016/j.jbc.2025.110509.
33. Sun, Y.; Pan, H.; He, Y.; Hu, C.; Gu, Y. Functional roles of the SHCBP1 and KIF23 interaction in modulating the cell-cycle and cisplatin resistance of head and neck squamous cell carcinoma. *Head Neck* **2022**, *44*, 591–605. https://doi.org/10.1002/hed.26961.
34. Zhang, Y.; Chen, L.; Wu, X.; Sun, Z.; Wang, F.; Wang, B.; Dong, P. The RNA N6-Methyladenosine Demethylase FTO Promotes Head and Neck Squamous Cell Carcinoma Proliferation and Migration by Increasing *CTNNB1*. *Int. J. Gen. Med.* **2021**, *14*, 8785–8795. https://doi.org/10.2147/IJGM.S339095.
35. Zheng, Y.; Fei, H. High Expression of E2F4 Is an Adverse Prognostic Factor and Related to Immune Infiltration in Oral Squamous Cell Carcinoma. *Biomed. Res. Int.* **2022**, *2022*, 4731364. https://doi.org/10.1155/2022/4731364.
36. Yang, S.; Sun, C.; Fang, Z.; Jin, H.; Li, C.; Zang, H.; Yang, L.; Li, L.; Saiyin, W. *CIAPIN1* as a Promoter of Oral Squamous Cell Carcinoma Progression. *J. Oral. Pathol. Med.* **2026**, *55*, 209–218. https://doi.org/10.1111/jop.70083.
37. Liu, P.; Wang, Y.; Li, X.; Liu, Z.; Sun, Y.; Liu, H.; Shao, Z.; Jiang, E.; Zhou, X.; Shang, Z. Enhanced lipid biosynthesis in oral squamous cell carcinoma cancer-associated fibroblasts contributes to tumor progression: Role of IL8/AKT/p-ACLY axis. *Cancer Sci.* **2024**, *115*, 1433–1445. https://doi.org/10.1111/cas.16111.

Disclaimer/Publisher's Note: The statements, opinions and data contained in all publications are solely those of the individual author(s) and contributor(s) and not of MDPI and/or the editor(s). MDPI and/or the editor(s) disclaim responsibility for any injury to people or property resulting from any ideas, methods, instructions or products referred to in the content.